

Probabilistic seismic demand assessment of self-centering concrete frames under mainshock-aftershock excitations

Long L. Song^{*1}, Tong Guo^{2a} and Xin Shi^{2b}

¹ College of Civil and Transportation Engineering, Hohai University, Nanjing, 210098, P.R. China

² Key Laboratory of Concrete and Prestressed Concrete Structures of the Ministry of Education, Southeast University, Nanjing, 210096, P.R. China

(Received August 20, 2018, Revised April 9, 2019, Accepted November 11, 2019)

Abstract. This paper investigates the effect of aftershocks on the seismic performance of self-centering (SC) prestressed concrete frames using the probabilistic seismic demand analysis methodology. For this purpose, a 4-story SC concrete frame and a conventional reinforced concrete (RC) frame are designed and numerically analyzed through nonlinear dynamic analyses based on a set of as-recorded mainshock-aftershock seismic sequences. The peak and residual story drifts are selected as the demand parameters. The probabilistic seismic demand models of the SC and RC frames are compared, and the SC frame is found to have less dispersion of peak and residual story drifts. The results of drift demand hazard analyses reveal that the SC frame experiences lower peak story drift hazards and significantly reduced residual story drift hazards than the RC frame when subjected to the mainshocks only or the mainshock-aftershock sequences, which demonstrates the advantages of the SC frame over the RC frame. For both the SC and RC frames, the influence of as-recorded aftershocks on the drift demand hazards is small. It is shown that artificial aftershocks can produce notably increased drift demand hazards of the RC frame, while the incremental effect of artificial aftershocks on the drift demand hazards of the SC frame is much smaller. It is also found that aftershock polarity does not influence the drift demand hazards of both the SC and RC frames.

Keywords: self-centering; concrete frame; aftershocks; probabilistic seismic demand analysis; residual drift

1. Introduction

Post-earthquake residual deformations of building structures after disastrous seismic events have gained much attention recently among the earthquake engineering and engineering seismology communities. The field surveys following the large earthquakes in China and around the world revealed significant financial losses of post-event repair/rebuild and building operation interruption, which result from the structural damage and associated residual deformations (Tsai *et al.* 2000, Zhao *et al.* 2009). For example, many damaged building structures in the 2011 Christchurch, New Zealand earthquake were demolished due to the uneconomically repair costs, although they did not suffer structural collapse (Bradley and Curbinovski 2011).

In order to reduce the residual deformations of building structures and therefore decrease the economic losses, studies during the past several decades focused on the development of many self-centering (SC) earthquake-resistant systems (Ricles *et al.* 2001, Christopoulos *et al.* 2002, Chou and Chen 2011, Vasdravellis *et al.* 2013, Clayton *et al.* 2013, Eatherton *et al.* 2014, Qiu and Zhu

2017, Xu *et al.* 2016, Chi *et al.* 2018, Rahman and Sritharan 2007, Kurama and Shen 2008, Guo *et al.* 2018, Cui *et al.* 2017, Morgen and Kurama 2004), which have the ability to significantly reduce the structural damage and residual deformations after strong earthquakes. Among these research efforts, self-centering concrete frames are being studied as alternatives to conventional monolithic reinforced concrete (RC) frames. Fig. 1 shows a schematic representation of a novel SC concrete frame, referred to herein as the self-centering prestressed concrete (SCPC) frame with web friction devices (WFDs), proposed by the authors (Song *et al.* 2014a). In the SCPC frame, elastic unbounded post-tensioned (PT) tendons run horizontally through the beams and columns to compress them together, and anchored to the exterior columns. The interface of the beam and column features gap opening and closing behavior under the seismic loading. The PT force in the tendons closes the gap that develops in earthquakes and returns the structure to its pre-earthquake vertical position (i.e., self-centering). The beam ends and column faces are armed with steel jackets and steel plates, respectively, to protect the concrete at the beam-column interfaces from damage. In order to improve the energy dissipation, web friction device (WFD), which consists of two steel channels connected to the column on either side of the beam, are installed in the vicinity of the beam-to-column connection. The webs of the two steel channels are compressed to the steel jacket using high-strength friction bolts, which provide the normal forces on the contact surfaces of the steel jacket

*Corresponding author, Lecturer,

E-mail: songll@hhu.edu.cn

^a Professor, E-mail: guotong@seu.edu.cn

^b Graduate Student, E-mail: 2381108948@qq.com

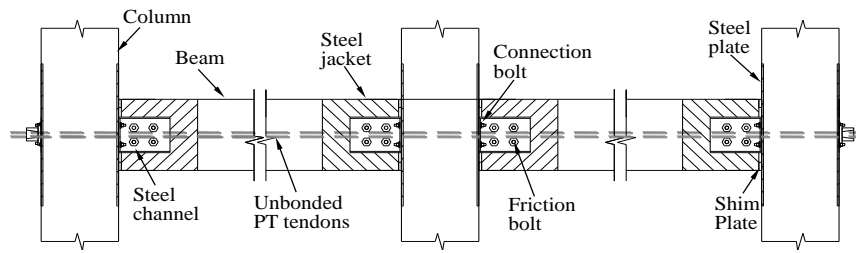
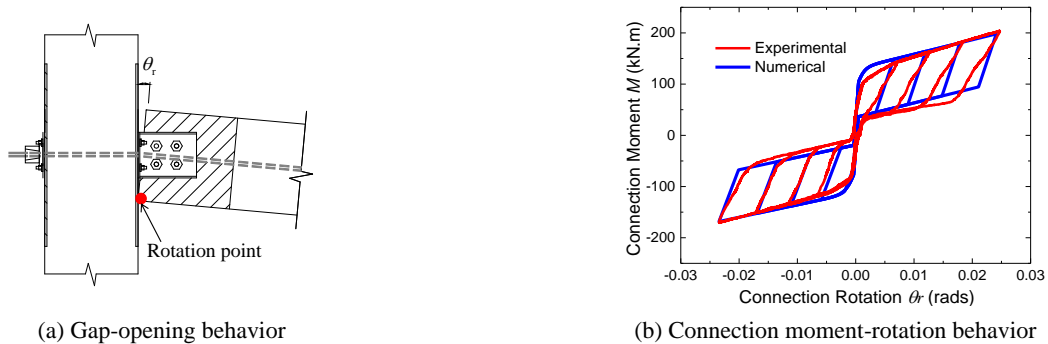


Fig. 1 SCPC frame with web friction devices (WFDs)



(a) Gap-opening behavior

(b) Connection moment-rotation behavior

Fig. 2 SCPC beam-column connection (Song *et al.* 2014a)

and steel channels. When the connection gap opens and closes under the earthquake loading, relative sliding motion occurs between the contact surfaces of the steel jacket and steel channels, and the earthquake energy can be dissipated through friction. The proposed frame system has been experimentally and analytically evaluated by static cyclic loading tests of SCPC beam-column connections (Song *et al.* 2014a) and 0.5-scale SCPC frame subassembly (Song *et al.* 2015a, Guo *et al.* 2016). Fig. 2 shows the obtained connection moment versus relative rotation behavior in the experiments of a SCPC beam-column connection with WFDs, which exhibits a stable flag-shaped hysteretic response with excellent self-centering capability and desirable energy dissipation. Due to the gap opening/closing mechanism at the beam-column interface and self-centering capability, the SCPC frame can experience large lateral displacements with the structural damage and residual deformations minimized.

Several research efforts (Morgen and Kurama 2008, Song *et al.* 2015b) have evaluated the seismic behavior of self-centering concrete frames compared with the conventional monolithic reinforced concrete (RC) frames through the nonlinear dynamic analysis method, using the ground motions scaled to the design basis earthquake (DBE) and maximum considered earthquake (MCE) hazard levels. More recently, Song and Guo (2017) evaluated the seismic performance of an SCPC frame by performing the seismic reliability analyses. However, the potential benefit of the self-centering concrete frame in mitigating the structural damage and residual drifts compared with the conventional RC frame has not yet been quantified probabilistically, which is important to demonstrate the efficacy of the self-centering concrete frame system.

In addition, building structures are usually subjected to a seismic sequence consisting of a mainshock and several

aftershocks in seismically active areas. During the past strong seismic events, such as the 1994 Northridge, California earthquake (McDonald *et al.* 2000) and the 1999 Chi-Chi, Taiwan earthquake (Kao and Chen 2000), it is observed that the structural damage of a building caused by the mainshock can be amplified by the aftershocks, and in some cases, the aftershocks could even lead to the collapse of mainshock-damaged building structures. Previous numerical investigations on the seismic performance of reinforced concrete (RC) frames also indicated that aftershocks could increase the vulnerability of structures (Hatzigeorgiou and Liolios 2010, Faisal *et al.* 2013, Song *et al.* 2014b). On the other hand, despite a relatively large amount of literature on the self-centering frames, their performance has not yet been evaluated probabilistically with the consideration of aftershocks. Therefore, incorporating the effect of aftershocks into the probabilistic performance evaluation procedure of SC concrete frames is needed, which would shed more insight on the potential advantages of the SC concrete frame system in comparison with the conventional RC frame system.

The objective of this paper is to compare the seismic performance of the SCPC frame with web friction devices (WFDs) and the conventional RC frame using the probabilistic seismic demand analysis (PSDA) procedure under the mainshock(MS)-aftershock(AS) seismic sequences. A total of 26 as-recorded MS-AS seismic sequences are selected for the nonlinear dynamic analyses of a 4-story SC concrete frame and a conventional RC frame, based on which the probabilistic seismic demand models of the SC and RC frames are established. The drift demand hazard curves are then constructed to compare the seismic performance of the RC and SC frames. Moreover, the effect of aftershock polarity on the drift demand hazards of the RC and SC frames is also investigated.

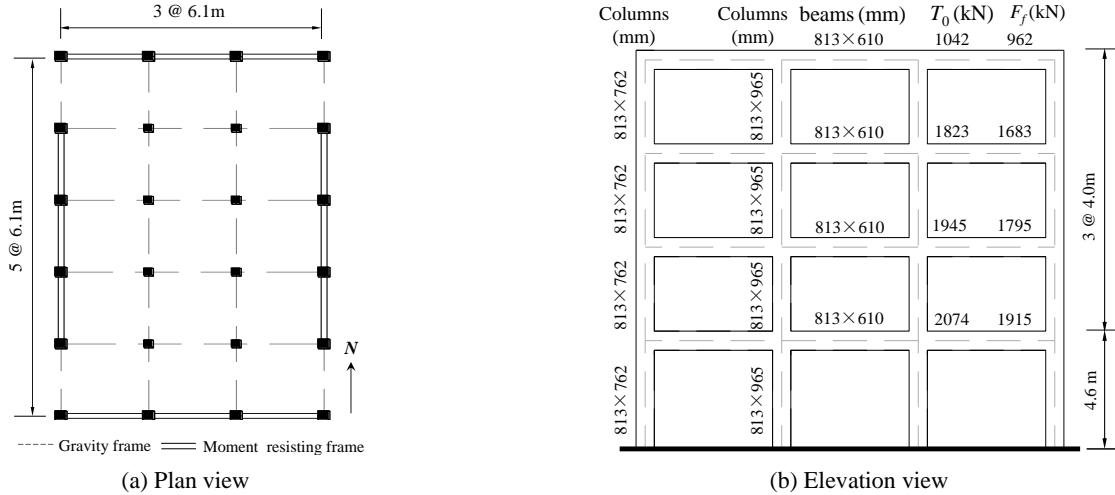


Fig. 3 Plan and elevation views of the case study frames

2. Case-study building structures

2.1 Design of the RC and SC frames

A 4-story RC frame building is used as the prototype structure in this study. This prototype RC frame was originally designed by Haselton and Deierlein (2007) to investigate the collapse risk of modern RC special moment-resisting frame (MRF) structures located in Los Angeles, California (34.1N, 118.5W). Fig. 3(a) shows the plan view of the prototype building. It is seen that the building consists of four identical three-bay MRFs along the perimeter of the building plan and the interior gravity frames. This study focuses on the response of a perimeter moment frame in the north-south (NS) direction. This RC moment frame is assumed to be in a stiff soil site and is designed in accordance with International Building Code (ICC 2003), the Minimum Design Loads for Buildings and Other Structures (ASCE 2002) and the Building Code Requirements for Reinforced Concrete (ACI 2002). The dead and live loads considered in design were 8.38 kN/m² and 2.39 kN/m², respectively. The cross-sectional dimensions of the beams and columns of the RC frame are shown in Fig. 3(b). The longitudinal reinforcement ratios for the exterior columns range from 1.0% (roof story) to 2.1% (first story), and from 1.0% to 1.6% for the interior columns. The average ratios of the beam top and bottom reinforcement range from 0.75% (roof floor) to 1.15% (first floor). Detailed information of the design parameters of the RC frame can be found in Haselton and Deierlein (2007).

For the sake of a direct comparison, the same beam/column cross-sectional dimensions and column reinforcement ratios are considered for the SC concrete frame and the prototype RC frame. The reinforcement ratios of the SC frame beams are assumed to be 0.5%, according to the suggestion in Song *et al.* (2014a). The design connection moment demand, M_d , of the SC frame are designed to be the mean value of positive and negative flexural strength at the RC frame beam ends. As shown in Fig. 4, M_d is the sum of moment induced by the initial PT force resultant in the beam, M_{T_0} , and moment induced by

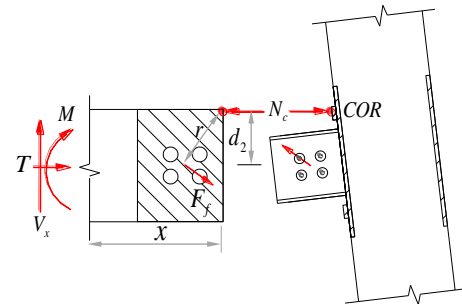


Fig. 4 Free-body diagram of SC beam-column connection

the friction force resultant in the WFD, M_{Ff} , as follows

$$M_d = M_{T_0} + M_{Ff} = T_0 \cdot d_2 + F_f \cdot r \quad (1)$$

where T_0 and F_f are the initial PT force resultant and the friction force resultant, respectively. d_2 and r are the distances from the center of rotation (COR) point to the beam section centroid and the friction force resultant, respectively. T_0 and F_f can be calculated according to Eq. (1) and the energy dissipation ratio of the SC beam-column connection, β_E , as follows

$$\beta_E = M_{Ff} / M_d \quad (2)$$

In this study, a value of 0.48 is assumed for β_E , and the calculated values of the design parameters T_0 and F_f for the SC concrete frame are shown in Fig. 3(b). With the T_0 determined, the area of PT tendons can be calculated assuming the design initial stress $f_{pi} = 0.50f_{py}$, where f_{py} = the design yield strength of PT tendons = 1675 MPa.

2.2 Numerical models

The 2D numerical models of the RC and SC frames are created using the finite element software OpenSees (Mazzoni *et al.* 2009). For both the RC and SC frames, leaning columns are used to consider the P-delta effects from the interior gravity frame system of the building (Song

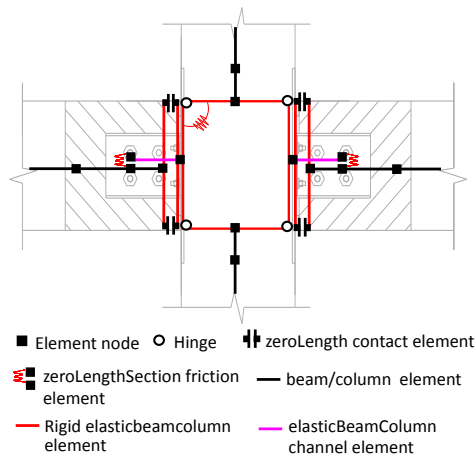


Fig. 5 Numerical model of SC beam-column connection

et al. 2015b). The foundation flexibility is considered by using a ZeroLength rotational spring at the column base, and the stiffness of the rotational spring is determined according to Haselton and Deierlein (2007). For the RC frame, elasticBeamColumn elements with concentrated plasticity hinges (Ibarra *et al.* 2005) at the element ends are used to model the beams. The beam element model parameters have been calibrated by Haselton *et al.* (2007) using the experimental results and have been used for the seismic response assessment of ductile RC frames (Fragiadakis *et al.* 2013, Bobadilla and Chopra 2008). An elastic joint shear spring is used to model the shear deformation in the panel zone. The nonlinear force Beam Column fiber elements, which can consider the interaction of axial load-flexural bending moment, are used to model the frame columns. The uniaxial Giuffrè-Menegotto-Pinto

Table 1 List of MS-AS sequences with the record sequence numbers (RSN) in the PEER NGA database

No.	Earthquake	Station name	RSN	M_w	Component	PGA(g)
1	Imperial Valley-6 1979	Calexico Fire Station	162	6.53	H-CXO225	0.28
			195	5.01	A-CXO225	0.10
2	Imperial Valley-6 1979	Calexico Fire Station	162	6.53	H-CXO315	0.20
			195	5.01	A-CXO315	0.07
3	Imperial Valley-6 1979	El Centro Array #11	174	6.53	H-E11140	0.37
			199	5.01	A-E11140	0.10
4	Imperial Valley-6 1979	El Centro Array #11	174	6.53	H-E11230	0.38
			199	5.01	A-E11230	0.19
5	Mammoth Lakes-01 1980	Long Valley Dam (Upr L Abut)	231	6.06	I-LUL000	0.43
			250	5.94	L-LUL000	0.95
6	Mammoth Lakes-01 1980	Long Valley Dam (Upr L Abut)	231	6.06	I-LUL090	0.27
			250	5.94	L-LUL090	0.41
7	Coalinga-01 1983	Pleasant Valley P.P.-yard	368	6.36	H-PVY045	0.60
			383	5.09	A-PVY045	0.10
8	Coalinga-01 1983	Pleasant Valley P.P. - yard	368	6.36	H-PVY135	0.53
			383	5.09	A-PVY135	0.21
9	Northridge-01 1994	Beverly Hills - 12520 Mulhol	952	6.69	MU2035	0.62
			1694	5.28	MU2035	0.15
10	Northridge-01 1994	Beverly Hills - 12520 Mulhol	952	6.69	MU2125	0.45
			1694	5.28	MU2125	0.17
11	Northridge-01 1994	Castaic - Old Ridge Route	963	6.69	ORR090	0.57
			1676	5.93	ORR090	0.14
12	Northridge-01 1994	Castaic - Old Ridge Route	963	6.69	ORR360	0.51
			1676	5.93	ORR360	0.12
13	Northridge-01 1994	LA - Hollywood Stor FF	995	6.69	PEL090	0.23
			1660	6.05	PEL090	0.16
14	Northridge-01 1994	LA - Hollywood Stor FF	995	6.69	PEL360	0.36
			1660	6.05	PEL360	0.17
15	Northridge-01 1994	Moorpark - Fire Sta	1039	6.69	MRP090	0.19
			1681	5.93	MRP090	0.14
16	Northridge-01 1994	Moorpark - Fire Sta	1039	6.69	MRP180	0.29
			1681	5.93	MRP180	0.18

Table 1 Continued

No.	Earthquake	Station name	RSN	M_w	Component	PGA(g)
17	Northridge-01 1994	Northridge - 17645 Saticoy St	1048	6.69	STC090	0.34
			1722	5.93	STC090	0.20
18	Northridge-01 1994	Northridge - 17645 Saticoy St	1048	6.69	STC180	0.46
			1722	5.28	STC180	0.18
19	Northridge-01 1994	Santa Monica City Hall	1077	6.69	STM090	0.88
			1730	5.28	STM090	0.10
20	Northridge-01 1994	Santa Monica City Hall	1077	6.69	STM360	0.37
			1730	5.28	STM180	0.08
21	Northridge-01 1994	Simi Valley - Katherine Rd	1080	6.69	KAT000	0.80
			1732	5.28	KAT000	0.08
22	Northridge-01 1994	Simi Valley - Katherine Rd	1080	6.69	KAT090	0.54
			1732	5.28	KAT090	0.10
23	Northridge-01 1994	Sun Valley - Roscoe Blvd	1082	6.69	RO3000	0.28
			1733	5.28	RO3000	0.14
24	Northridge-01 1994	Sun Valley - Roscoe Blvd	1082	6.69	RO3090	0.45
			1733	5.28	RO3090	0.10
25	Chi-Chi_ Taiwan 1999	CHY041	1205	7.62	CHY041-E	0.30
			3278	6.3	CHY041E	0.16
26	Chi-Chi_ Taiwan 1999	CHY041	1205	7.62	CHY041-N	0.64
			3278	6.3	HY041N	0.18

model and Kent-Scott-Park model in OpenSees are used to model the steel reinforcement and concrete, respectively.

For the SC frame, both the beams and columns are modeled using the nonlinear forceBeamColumn fiber elements, as can be seen in the numerical model of SC beam-column connection (Fig. 5). ZeroLength contact elements with compression-only behavior, placed at the center of rotation (COR) points, are used to model the connection gap opening and closing. The steel channel is modeled by an elastic Beam Column element, while the friction force resultant in the WFD is modeled by a zeroLengthSection element. The beam-column joint panel deformation is simulated using a zeroLength element with bilinear elastic rotational behavior. The PT tendon is simulated using a truss element with initial strain. The comparison of the obtained connection moment versus relative rotation relationships from the numerical model and test results can be seen in Fig. 2(b), which shows a good agreement between the numerical and experimental results. Further information of the RC and SC frame models can also be found in Song *et al.* (2015b).

The nonlinear time-history analyses are conducted assuming a 5% Rayleigh damping ratio for the first and third vibration modes. To capture the residual displacements accurately, each analysis is conducted with additional zero acceleration values (20 s) padded to the mainshock and aftershock acceleration time-histories. According to the modal analysis results, the fundamental periods of vibration of the RC and SC frames are 0.90 s and 0.81 s, respectively.

3. Earthquake ground motions

A suite of 26 far-fault as-recorded mainshock(MS)-aftershock (AS) ground motion sequences from two orthogonal horizontal directions are selected from the Pacific Earthquake Engineering Research (PEER) NGA database (Ancheta *et al.* 2014) for nonlinear dynamic analysis. The classification of the far-fault records consists with criteria in FEMA-P695 (FEMA 2009). The selection criteria for the mainshocks and aftershocks are similar to those used by Song *et al.* (2014b). Every seismic sequence includes a mainshock event and a corresponding aftershock event at the same station with the site soil condition similar to that at the prototype building site. The moment magnitudes (M_w) of the mainshock and aftershock are no less than 5.0 and the peak ground acceleration (PGA) values of the ground motions are no less than 0.5 g. Table 1 summarizes the characteristics of the as-recorded MS-AS ground motion sequences for use in this study. Fig. 6 shows the 5% damped response spectra of the mainshocks and aftershocks.

4. Structural responses under individual seismic sequences

To understand the influence of aftershocks on the seismic behaviors of the RC and SC frames, roof drift time-history results of the two frames under the as-recorded sequences in Table 1 are compared, and some typical results are presented. Fig. 7(a) shows the roof drift responses of the

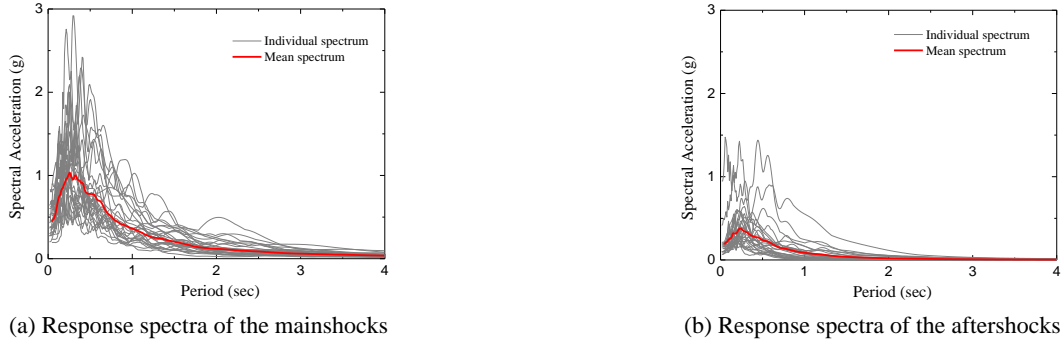


Fig. 6 Response spectra of the as-recorded mainshocks and aftershocks

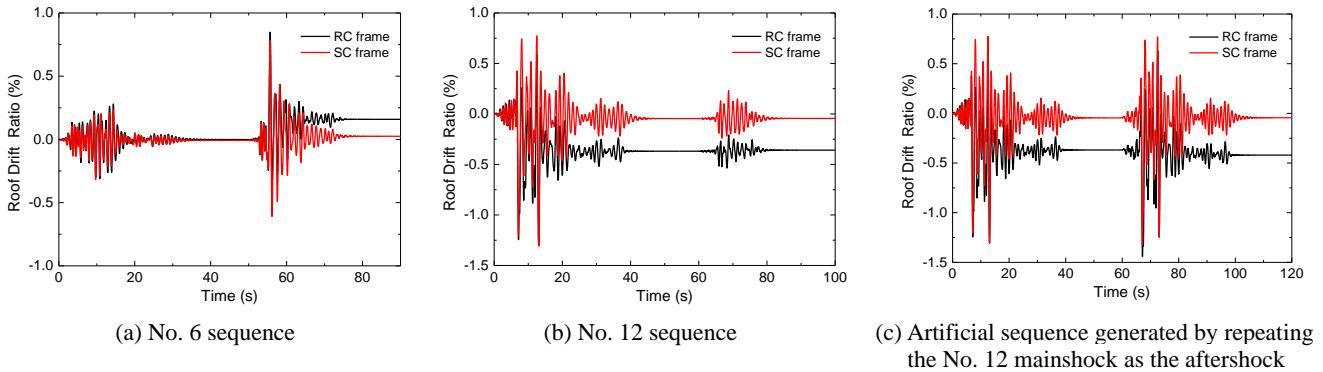


Fig. 7 Roof drift time-histories of the RC and SC frames

RC and SC frames subjected to the No. 6 as-recorded sequence, of which the PGA of the aftershock is larger than that of the mainshock. For both the RC and SC frames, the aftershock of the No. 6 sequence increase the peak and residual roof drift demands caused by the mainshock. Therefore, the structural demands of the RC and SC frames may be underestimated when only the mainshock is considered. It is also observed that the peak roof drifts of the two frames are similar. The residual roof drifts of the RC and SC frames at the end of the mainshock are minimal. However, at the end of the aftershock, the residual roof drift of the RC frame is 0.16%, and the residual roof drift of the SC frame is much less, being 0.02%.

Fig. 7(b) shows the roof drift time-histories of the RC and SC frames under the No. 12 as-recorded sequence. It is observed that that the aftershock of the No. 12 sequence does not increase the peak and residual drift demands of the RC and SC frames triggered by the mainshock. It should be noted that this phenomenon is valid among the analysis results of most of the as-recorded MS-AS sequences in Table 1.

Previous studies (Hatzigeorgiou and Liolios 2010, Faisal *et al.* 2013) have also used the artificial seismic sequences on the response assessment of structures, so it is worthy to compare the drift demands of the RC and SC frames under the artificial sequence. Fig. 7(c) shows the roof drift responses of the RC and SC frames subjected to the artificial sequence generated by repeating the mainshock of the No. 12 sequence as the aftershock. It can be seen that the peak and residual roof drifts of the RC frame under the artificial sequence are higher than those induced by the

mainshock only. For the SC frame, however, the incremental effect of artificial aftershock on the roof drift demands is negligible.

5. Probabilistic seismic demand analysis (PSDA)

5.1 PSDA methodology

The probabilistic seismic demand analysis (PSDA) methodology usually provides the hazard curve of the engineering demand parameter (EDP), in which the mean annual frequency (MAF) of a specific demand level is given. According to Deierlein *et al.* (2003), the demand hazard can be calculated as

$$\lambda_{EDP}(y) = \int P(EDP > y | SI = x) dH_{SI}(x) \quad (3)$$

where $\lambda_{EDP}(y)$ denotes the MAF of the EDP exceeding the value y ; $P(EDP > y | SI = x)$ is the probability that the EDP exceeds the value y , conditioned on the seismic intensity (SI) equal to the value x ; $H_{SI}(x)$ is the seismic hazard represented by the annual frequency of the SI exceeding the value x and can be calculated using (Cornell *et al.* 2002)

$$H_{SI}(x) = k_0 x^{-k} \quad (4)$$

where the constants k_0 and k depend on the region and site condition of the structure, and can be obtained by fitting the function to the seismic hazard analysis results around the

return periods of interest.

Assuming that the distribution of the EDP is log-normal, which is confirmed in many previous studies (Song and Ellingwood 1999), $P(EDP > y|SI = x)$ can be expressed as

$$P(EDP > y|SI = x) = 1 - \Phi \left[\frac{\ln(y) - \ln(m_{EDP|SI})}{\beta_{EDP|SI}} \right] \quad (5)$$

where Φ is the standard normal cumulative distribution integral function; $m_{EDP|SI}$ and $\beta_{EDP|SI}$ are the median and dispersion values of the structural demand, respectively.

The relation between the structural demand and the seismic intensity of earthquake, which is commonly referred as the probabilistic seismic demand model, can be established using the power-law function (Cornell *et al.* 2002)

$$EDP = a(SI)^b \quad (6)$$

Therefore, a linear relationship can be obtained between the median demand and the seismic intensity in the log-log space, as follows

$$\ln(EDP) = \ln(a) + b \ln(SI) \quad (7)$$

By making a log-log linear regression analysis between the structural demand and seismic intensity from the nonlinear dynamic analysis results of N earthquake ground motions, the values of coefficients a and b can be obtained and the dispersion value $\beta_{EDP|SI}$ can be calculated as

$$\beta_{EDP|SI} = \sqrt{\frac{\sum_{i=1}^N [\ln(EDP_i) - \ln(aSI_i^b)]^2}{N - 2}} \quad (8)$$

Based on Eqs. (4)-(8), Eq. (3) can be rewritten as the following equation (Cornell *et al.* 2002)

$$\lambda_{EDP}(y) = k_0 \left[\left(\frac{y}{a} \right)^{\frac{1}{b}} \right]^{-k} \exp \left(\frac{k^2}{2b^2} \beta_{EDP|SI}^2 \right) \quad (9)$$

5.2 Probabilistic seismic demand model

In this study, the peak story drift (PSD) and residual story drift (RSD) are selected as the engineering demand parameters (EDPs), whereas the elastic spectral acceleration at the fundamental mode period $S_a(T_1)$ is used as the seismic intensity (SI) measure. To get sufficient data in the development of the probabilistic seismic demand model, incremental dynamic analysis (IDA) is performed by scaling the mean $S_a(T_1)$ of the two orthogonal mainshock components at the same station to increasing intensity levels. It should be noted that for each level of mainshock-aftershock analysis, the intensity ratio of the mainshock and the aftershock remains the same as that for the unscaled mainshock-aftershock sequence.

Fig. 8 shows the seismic demands of the RC and SC frames under the mainshocks only, as-recorded mainshock-aftershock sequences and artificial mainshock-aftershock sequences. The values of the regression parameters $\ln(a)$ and b in Eq. (7), along with the dispersion of demands, $\beta_{EDP|SI}$, from the log-log linear regression analysis results are shown in Table 2. It is observed that the dispersion values of the peak and residual story drift demands for the SC frame are smaller than those for the RC frame. The much smaller values of the parameters $\ln(a)$ and b for the SC frame in terms of residual story drifts reveal that the SC frame is very effective in mitigating the residual deformations.

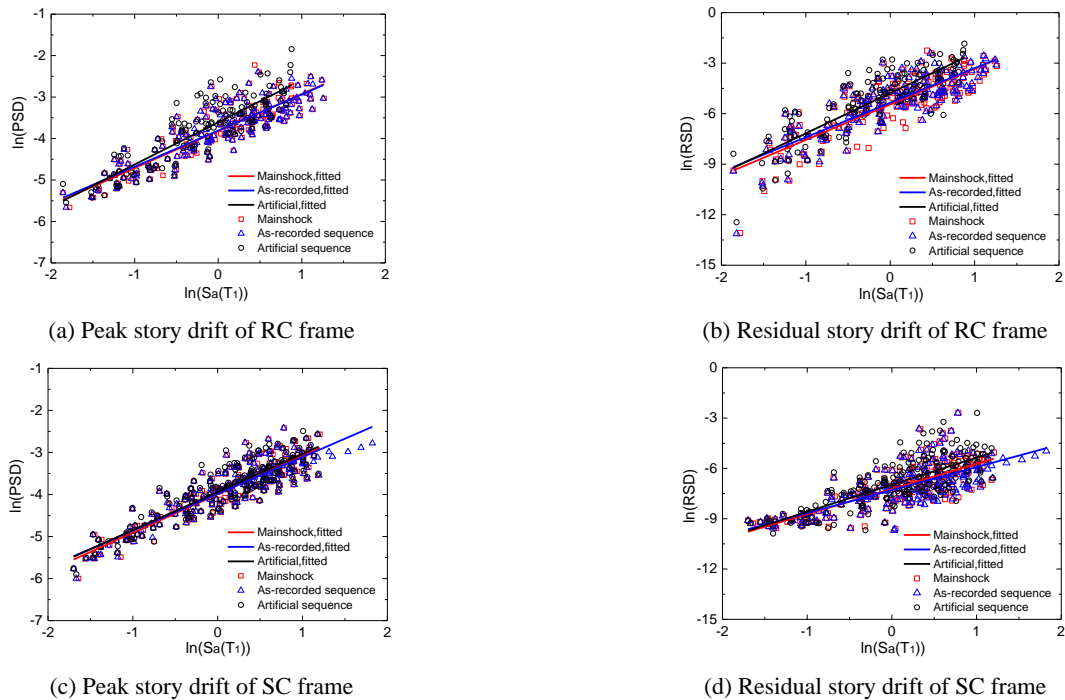


Fig. 8 Seismic demands of the RC and SC frames

Table 2 Probabilistic seismic demand models for the RC and SC frames

Frame	Ground motion	Peak story drift			Residual story drift		
		$\ln(a)$	b	$\beta_{EDP/SI}$	$\ln(a)$	b	$\beta_{EDP/SI}$
RC	Mainshock	-3.8194	0.8921	0.3455	-5.4491	2.1107	0.9933
	As-recorded sequence	-3.8077	0.8719	0.3396	-5.3496	2.0548	0.9592
	Artificial sequence	-3.6079	1.0187	0.3909	-4.7807	2.3875	1.0294
SC	Mainshock	-3.9932	0.9145	0.3115	-7.2225	1.5015	0.9058
	As-recorded sequence	-3.9846	0.8749	0.3137	-7.2934	1.3717	0.9173
	Artificial sequence	-3.9399	0.9065	0.3085	-6.9696	1.6135	0.9070

In general, for both the RC and SC frames, the fitted lines of the analysis results between considering the mainshocks only and as-recorded mainshock-aftershock sequences are close. In particular, due to the excellent self-centering capability, the residual drift demands of the SC frame caused by the as-recorded sequences are slightly smaller than those caused by the mainshocks only, which is evidenced by smaller values of $\ln(a)$ and b for the as-recorded sequences, as shown in Table 2.

It is observed from Fig. 8(a) that the artificial mainshock-aftershock sequences result in larger peak story drift demands of the RC frame than those produced by the as-recorded sequences. However, the artificial and as-recorded sequences produce similar peak story drift demands of SC frame, as can be seen in Fig. 8(c). Comparison of the data in Figs. 8(b) and (d) reveals that the incremental effect the artificial aftershocks on the residual story drift demands is less pronounced for the SC frame than for the RC frame.

5.3 Seismic hazard curves

The seismic hazard curve provides the annual probability of exceeding a specific seismic intensity (SI) value for a given site. The USGS (2018) website provides the relationships between the probability of exceedance (PE) in 50 years and the 5% damped spectral acceleration (S_a) with different fundamental periods, which can be used to construct the seismic hazard curves of the RC and SC frames, as shown in Fig. 9. These curves are obtained by fitting a line using Eq. (4) to the three points defined by the annual PE (i.e., 1/72, 1/475, and 1/2475, corresponding to 2%, 10%, and 50% PE in 50 years, respectively) and corresponding spectral accelerations at the fundamental periods of the RC and SC frames. Fig. 9 also shows the values of parameters k_0 and k obtained from the least-squares regression analyses.

5.4 Drift demand hazard curves

Using the probabilistic seismic demand models in Table 2 and the seismic hazard curves in Fig. 9, the drift demand hazard curves of the RC and SC frames can be obtained by Eq. (9). Fig. 10 shows the peak and residual story drift hazard curves, and Table 3 presents the peak and residual story drifts corresponding to different probability of exceedance (PE) in 50 years.

It is seen from Fig. 10(a) that the SC frame has smaller peak story drift hazards than the RC frame for the mainshocks only and the as-recorded sequences, which can also be evidenced by the smaller peak story drifts experienced by the SC frame for a given hazard level. For example, the peak story drifts corresponding to 2% PE in 50

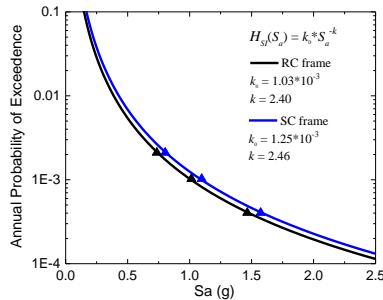


Fig. 9 Spectral acceleration hazard curves for the RC and SC frames

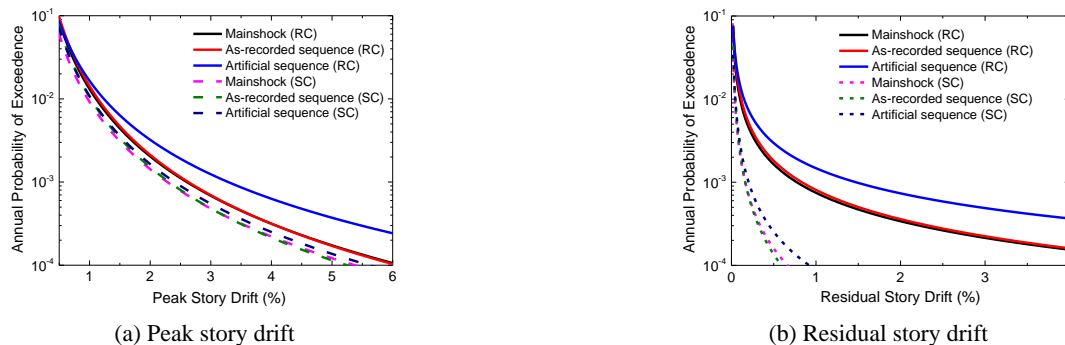


Fig. 10 Annual hazard curves for peak and residual story drifts of the RC and SC frames

Table 3 Peak and residual story drifts corresponding to different PE in 50 years

PE in 50 yr. (Annual PE)	Ground motion	Peak story drift		Residual story drift	
		RC frame	SC frame	RC frame	SC frame
10% (1/475)	Mainshock	0.0197	0.0173	0.0040	0.0010
	As-recorded sequence	0.0201	0.0177	0.0044	0.0011
	Artificial sequence	0.0240	0.0183	0.0070	0.0012
2% (1/2475)	Mainshock	0.0365	0.0320	0.0172	0.0028
	As-recorded sequence	0.0366	0.0319	0.0181	0.0027
	Artificial sequence	0.0483	0.0336	0.0363	0.0037

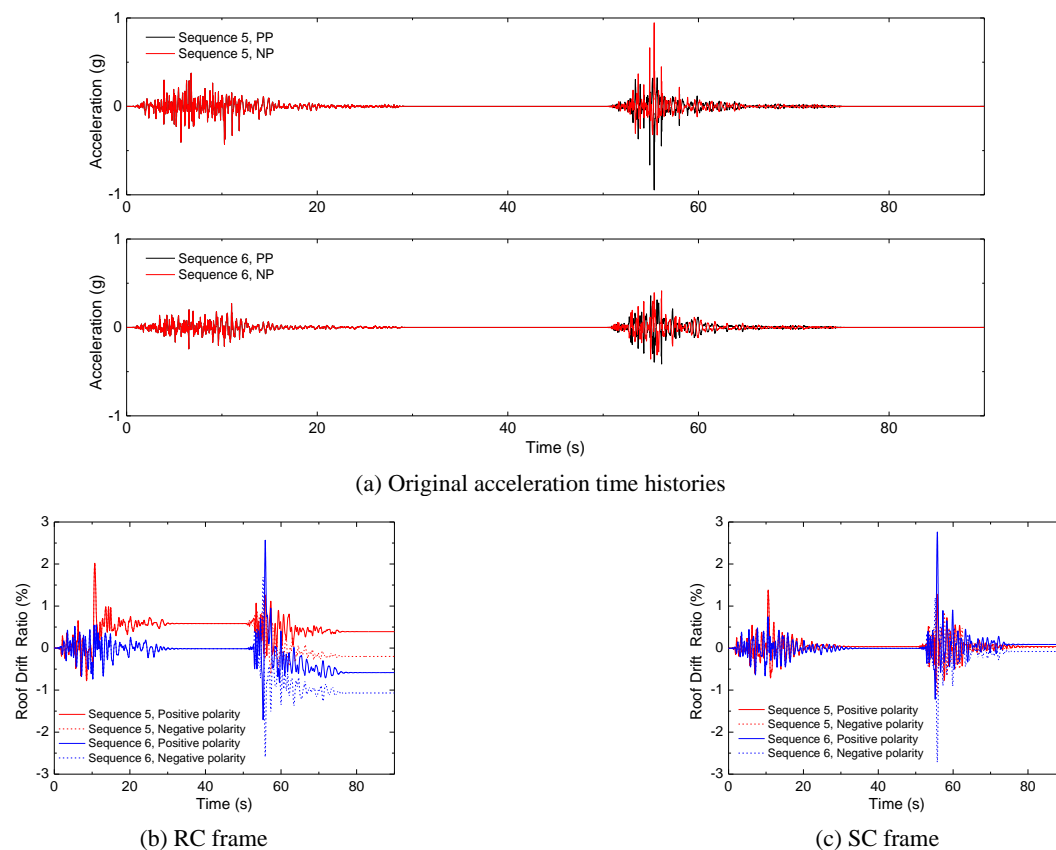


Fig. 11 Roof drift time-histories of the RC and SC frames under the No. 5 and 6 sequences with different aftershock polarity

years for the SC frame subjected to mainshocks only and the as-recorded sequences are 12.3% and 12.8% smaller than those for the RC frame. For both the RC and SC frames, the difference between the peak story drift hazard curves of the mainshocks only and the as-recorded sequences is insignificant. By comparing the hazard curves of mainshocks only and the artificial sequences, it is seen that the artificial sequences lead to higher peak story drift hazards of the RC frame. On the other hand, the effect of artificial sequences on the increase of peak story drift hazards of the SC frame is much smaller. Compared with the mainshocks only, the artificial sequences produce 21.8% and 32.3% higher peak story drift demands corresponding to 10% and 2% PE in 50 years for the RC frame, while the values for the SC frame are 5.8% and 5.0%.

Fig. 10(b) shows the residual story drift hazard curves of

the RC and SC frames. It can be seen that the SC frame experiences much reduced hazards of residual story drift as compared with the RC frame. When subjected to the mainshocks only, the residual story drifts of the RC frame corresponding to 10% and 2% PE in 50 years are 0.40% and 1.72%, respectively, while the values of the SC frame are much smaller, i.e., 0.10% and 0.28%, respectively. Similar to the observation in the peak story drift hazard curves, the effect of as-recorded aftershocks on the residual story drift hazards in very small for both the RC and SC frames. When subjected to the artificial sequences, the RC frame experiences significantly higher residual story drift hazards as compared with those caused by the mainshocks only, while the incremental effect of artificial aftershocks on the residual story drift hazards of the SC frame is much smaller. Compared to the residual story drifts under the mainshocks

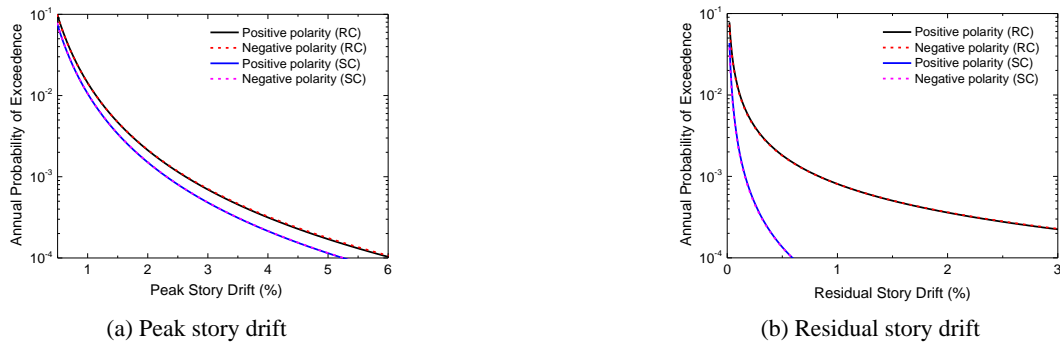


Fig. 12 Annual hazard curves for peak and residual story drifts considering aftershock polarity

only, the residual story drifts corresponding to 10% and 2% PE in 50 years for the RC frame under the artificial sequences are increased by 75% and 111%, respectively, while the increases are considerably lower for the SC frame, being 20% and 32%, respectively.

5.5 Influence of aftershock polarity

The aftershock polarity refers to the direction of aftershock in respect of mainshock in a mainshock-aftershock sequence (Raghunandan *et al.* 2012). As shown in Fig. 11(a), the aftershock with positive polarity (PP) refers to the aftershock applied in the same direction of the original mainshock, while in the negative polarity (NP) case, the aftershock is applied in the opposite direction of the original mainshock. To illustrate the effect of aftershock polarity on the seismic responses, Figs. 11(b)-(c) show the roof drift time-histories of the RC and SC frames under the No. 5 and 6 sequences, with the mean $S_a(T_1)$ of the two orthogonal mainshock components scaled to 0.9 g.

For the RC frame under the No. 5 seismic sequence, both the positive and negative aftershock polarities lead to a re-centering behavior, and the aftershock with positive polarity reduces the 0.58% post-mainshock residual roof drift to 0.39%, while the aftershock with negative polarity produces a residual roof drift of 0.20% in the opposite direction. On the other hand, both the positive and negative aftershock polarities lead to higher peak and residual roof drifts of the RC frame under the No. 6 seismic sequence as compared with those induced by the mainshock only. In addition, although the residual roof drift of the RC frame at the end of the No. 6 mainshock is minimal, the residual roof drifts induced by the No. 6 aftershocks with positive and negative polarities are different (i.e., 0.58% for the positive polarity and 1.1% for the negative polarity, respectively). This can be explained that, due to the non-ignorable transient drift demands experienced during the mainshock, the RC frame may have some structural damage at the end of the mainshock, even if the post-mainshock residual drift is small.

For the SC frame, however, due to that the gap-opening behavior is allowed at the beam-column interfaces, it can withstand large drift demands without yielding the structural members at the beam-column regions. Therefore, under the No. 5 and 6 sequences, the SC frame experiences minimal residual roof drifts at the end of mainshocks, and

the peak or residual roof drifts caused by the aftershocks with positive and negative polarities are very close, as shown in Fig. 11(c).

To further study the effect of aftershock polarity on the drift hazard curves, Fig. 12 shows the peak and residual story drift hazard curves of the RC and SC frames under the as-recorded seismic sequences with different polarities. For both the RC and SC frames, it is found that the peak/residual story drift demand hazard curves between considering the positive and negative aftershock polarities are essentially the same. This finding underscores the importance of considering the aftershock polarity in developing drift hazard estimates for the conventional RC and SC frames.

6. Conclusions

An innovative self-centering (SC) concrete frame system, which incorporates the self-centering prestressed concrete (SCPC) beam-column connections, had been previously developed as an alternative to the conventional reinforced concrete (RC) frame system. This SC frame system aims to use the unbounded post-tensioned (PT) tendons to reduce the residual displacements, and the web friction devices to increase the energy dissipation, thus controlling the peak displacements. To demonstrate the effectiveness of this new SC concrete frame system, a comparative assessment of the seismic performance of a 4-story SC concrete frame and a conventional RC frame under mainshock-aftershock seismic sequences is performed using the probabilistic seismic demand analysis methodology. A suite of 26 far-fault as-recorded mainshock-aftershock seismic sequences are selected and nonlinear dynamic analyses are conducted on the RC and SC frames to obtain the structural demands. Then, the probabilistic seismic demand models and demand hazard curves in terms of peak and residual story drifts are constructed for both the RC and SC frames. In addition, the effect of aftershock polarity on the performance of the RC and SC frames is investigated. According to the analysis results of this study, the following conclusions can be obtained:

- (1) Nonlinear dynamic analysis results of the RC and SC frames under the as-recorded mainshock-aftershock sequences reveal that aftershocks may

produce higher peak and residual drift demands of the RC and SC frames in some cases when the aftershock is more intense than the mainshock.

- (2) The comparison of the probabilistic seismic demand models of the RC and SC frames reveals that the dispersion values of peak and residual story drift demands for the SC frame are smaller than those for the RC frame.
- (3) The comparison of the story drift hazard curves of the RC and SC frames reveals that the SC frame has lower peak story drift hazards and much smaller residual story drift hazards than the RC frame under the mainshocks only or the mainshock-aftershock sequences, which demonstrates the benefits of the SC frame over the RC frame.
- (4) By comparing the analysis results of the mainshocks only and as-recorded seismic sequences, it is found that the incremental effect of the as-recorded aftershocks on the drift hazards of the RC and SC frames is generally minimal.
- (5) Compared with the mainshocks only, the artificial sequences can significantly increase the peak and residual story drift hazards of the RC frame. On the other hand, the increase of peak story drift hazard for the SC frame due to the artificial aftershocks is very limited, and the incremental effect of artificial aftershocks on the residual story drift hazard is much smaller for the SC frame than for the RC frame.
- (6) The analysis results for the as-recorded sequences with different polarities reveal that the aftershock polarity has essentially no influence on the peak/residual story drift hazards of the RC and SC frames.

It should be noted that only one SC frame and one conventional RC frame are comparatively evaluated in the present study, further investigations using structural models with different heights and design parameters may get more general results.

Acknowledgments

The support from: (1) the National Natural Science Foundation of China under Grants No. 51708172; (2) the Natural Science Foundation of Jiangsu Province under Grant BK20170890; and (3) the project funded by China Postdoctoral Science Foundation under Grant 2019M651674 is gratefully acknowledged.

References

ACI 318-02 (2002), Building Code Requirements for Reinforced Concrete, American Concrete Institute; Farmington Hills, MI, USA.

ASCE 7-02 (2002), Minimum Design Loads for Buildings and Other Structures, American Society of Civil Engineers (ASCE), Reston, VA, USA.

Ancheta, T.D., Darragh, R.B., Stewart, J.P., Seyhan, E., Silva,

W.J., Chiou, B., Wooddell, K.E., Graves, R.W., Kottke, A.R., Boore, D.M., Kishida, T. and Donahue, J.L. (2014), "NGA-West2 Database", *Earthq. Spec.*, **30**, 989-1005. <https://doi.org/10.1193/070913EQS197M>

Bobadilla, H. and Chopra, A.K. (2008), "Evaluation of the MPA procedure for estimating seismic demands: RC-SMRF buildings", *Earthq. Spec.*, **24**(4), 827-845. <https://doi.org/10.1193/1.2945295>

Bradley, B.A. and Curbinovski, M. (2011), "Near-source strong ground motions observed in the 22 February 2011 Christchurch earthquake", *Seismol. Res. Lett.*, **82**(6), 853-865. <https://doi.org/10.1785/gssrl.82.6.853>

Chi, P., Guo, T., Peng, Y., Cao, D. and Dong, J. (2018), "Development of a self-centering tension-only brace for seismic protection of frame structures", *Steel Compos. Struct., Int. J.*, **26**(5), 573-582. <https://doi.org/10.12989/scs.2018.26.5.573>

Chou, C.C. and Chen, J.H. (2011), "Seismic design and shake table tests of a steel post-tensioned self-centering moment frame with a slab accommodating frame expansion", *Earthq. Eng. Struct. Dyn.*, **40**(11), 1241-1261. <https://doi.org/10.1002/eqe.1086>

Christopoulos, C., Filiatrault, A., Uang, C.M. and Folz, B. (2002), "Posttensioned energy dissipating connections for moment-resisting steel frames", *J. Struct. Eng.*, **128**(9), 1111-1120. [https://doi.org/10.1061/\(ASCE\)0733-9445\(2002\)128:9\(1111\)](https://doi.org/10.1061/(ASCE)0733-9445(2002)128:9(1111))

Clayton, P.M., Berman, J.W. and Lowes, L.N. (2013), "Subassembly testing and modeling of self-centering steel plate shear walls", *Eng. Struct.*, **56**, 1848-1857. <https://doi.org/10.1016/j.engstruct.2013.06.030>

Cornell, C., Jalayer, F., Hamburger, R. and Foutch, D. (2002), "Probabilistic basis for 2000 SAC Federal Emergency Management Agency steel moment frame guidelines", *J. Struct. Eng.*, **128**(4), 526-533. [https://doi.org/10.1061/\(ASCE\)0733-9445\(2002\)128:4\(526\)](https://doi.org/10.1061/(ASCE)0733-9445(2002)128:4(526))

Cui, Y., Lu, X. and Jiang, C. (2017), "Experimental investigation of tri-axial self-centering reinforced concrete frame structures through shaking table tests", *Eng. Struct.*, **132**, 684-694. <https://doi.org/10.1016/j.engstruct.2016.11.066>

Deierlein, G.G., Krawinkler, H. and Cornell, C.A. (2003), "A framework for performance-based earthquake engineering", *Pacific Conference on Earthquake Engineering*, Christchurch, New Zealand.

Eatherton, M., Ma, X., Krawinkler, H., Deierlein, G.G. and Hajjar, J.F. (2014), "Quasi-static cyclic behavior of controlled rocking steel frames", *J. Struct. Eng.*, **140**(11), 04014083. [https://doi.org/10.1061/\(ASCE\)ST.1943-541X.0001005](https://doi.org/10.1061/(ASCE)ST.1943-541X.0001005)

Faisal, A., Majid, T.A. and Hatzigeorgiou, G.D. (2013), "Investigation of story ductility demands of inelastic concrete frames subjected to repeated earthquakes", *Soil Dyn. Earthq. Eng.*, **44**, 42-53. <https://doi.org/10.1016/j.soildyn.2012.08.012>

FEMA-P695 (2009), Quantification of Building Seismic Performance Factors, Federal Emergency Management Agency (FEMA), Washington D.C., USA.

Fragiadakis, M., Vamvatsikos, D. and Aschheim, M. (2013), "Application of nonlinear static procedures for seismic assessment of regular RC moment frame buildings", *Earthq. Spec.*, **30**(2), 767-794. <https://doi.org/10.1193/111511EQS281M>

Guo, T., Song, L.L., Cao, Z.L. and Gu, Y. (2016), "Large-scale tests on cyclic behavior of self-centering prestressed concrete frames", *ACI Struct. J.*, **113**(6), 1263-1274. <https://doi.org/10.14359/51689248>

Guo, T., Wang, L., Xu, Z. and Hao, Y.W. (2018), "Experimental and numerical investigation of jointed self-centering concrete walls with friction connectors", *Eng. Struct.*, **161**, 192-206. <https://doi.org/10.1016/j.engstruct.2018.02.028>

Haselton, C.B. and Deierlein, G.G. (2007), "Assessing seismic

- collapse safety of modern reinforced concrete moment frame buildings”, Report No. 156, John A. Blume Earthquake Engineering Center, Stanford University, USA.
- Haselton, C.B., Liel, A.B., Lange, S.T. and Deierlein, G.G. (2007), “Beam-column element model calibrated for predicting flexural response leading to global collapse of RC frame buildings”, Report no. 2007/03, Pacific Earthquake Engineering Research Center, University of California, USA.
- Hatzigeorgiou, G.D. and Liolios, A.A. (2010), “Nonlinear behaviour of RC frames under repeated strong ground motions”, *Soil Dyn. Earthq. Eng.*, **30**(10), 1010-1025. <https://doi.org/10.1016/j.soildyn.2010.04.013>
- Ibarra, L.F., Medina, R.A. and Krawinkler, H. (2005), “Hysteretic models that incorporate strength and stiffness deterioration”, *Earthq. Eng. Struct. Dyn.*, **34**, 1489-1511. <https://doi.org/10.1002/eqe.495>
- IBC-2003 (2003), International Building Code, International Code Council (ICC), Falls Church, VA, USA.
- Kao, H. and Chen, W.P. (2000), “The Chi-Chi earthquake sequence: Active, out-of-sequence thrust faulting in Taiwan”, *Science*, **288**(5475), 2346-2349. <https://doi.org/10.1126/science.288.5475.2346>
- Kurama, Y.C. and Shen, Q. (2008), “Seismic design and response evaluation of unbonded post-tensioned hybrid coupled wall structures”, *Earthq. Eng. Struct. Dyn.*, **37**(14), 1677-1702. <https://doi.org/10.1002/eqe.852>
- Mazzoni, S., McKenna, F., Scott, M.H. and Fenves, G.L. (2009), OpenSees (Open system for earthquake engineering simulation), Pacific Earthquake Engineering Research (PEER) Center, University of California, Berkeley, CA, USA.
- McDonald, B., Bozorgnia, Y. and Osteraas, J. (2000), “Structural damage claims attributed to aftershocks”, *Proceedings: Second Congress Forensic Engineering, American Society of Civil Engineers*, San Juan, Puerto Rico, USA.
- Morgen, B.G. and Kurama, Y.C. (2004), “A friction damper for post-tensioned precast concrete moment frames”, *PCI J.*, **49**(4), <https://doi.org/10.1126/pci.07012004.112.133>
- Morgen, B.G. and Kurama, Y.C. (2008), “Seismic response evaluation of posttensioned precast concrete frames with friction dampers”, *J. Struct. Eng.*, **134** (1), 132-145. [https://doi.org/10.1061/\(ASCE\)0733-9445\(2008\)134:1\(132\)](https://doi.org/10.1061/(ASCE)0733-9445(2008)134:1(132))
- Qiu, C.X. and Zhu, S. (2017), “Performance-based seismic design of self-centering steel frames with SMA-based braces”, *Eng. Struct.*, **130**, 67-82. [https://doi.org/10.1061/\(ASCE\)0733-9445\(2008\)134:1\(132\)](https://doi.org/10.1061/(ASCE)0733-9445(2008)134:1(132))
- Raghunandan, M., Liel, A.B., Ryu, H., Luco, N. and Uma, S.R. (2012), “Aftershock fragility curves and tagging assessments for a mainshock-damaged building”, *Proceedings of the 15th World Conference on Earthquake Engineering*, Lisbon, Portugal.
- Rahman, M.A. and Sritharan, S. (2007), “Performance-based seismic evaluation of two five-story precast concrete hybrid frame buildings”, *J. Struct. Eng.*, **133**, 1489-1500. [https://doi.org/10.1061/\(ASCE\)0733-9445\(2007\)133:11\(1489\)](https://doi.org/10.1061/(ASCE)0733-9445(2007)133:11(1489))
- Ricles, J.M., Sause, R. and Garlock, M.M. (2001), “Posttensioned seismic-resistant connections for steel frames”, *J. Struct. Eng.*, **127**(2), 113-121. [https://doi.org/10.1061/\(ASCE\)0733-9445\(2001\)127:2\(113\)](https://doi.org/10.1061/(ASCE)0733-9445(2001)127:2(113))
- Song, J. and Ellingwood, B.R. (1999), “Seismic reliability of special moment steel frames with welded connections: II”, *J. Struct. Eng.*, **125**(4), 372-384. [https://doi.org/10.1061/\(ASCE\)0733-9445\(1999\)125:4\(372\)](https://doi.org/10.1061/(ASCE)0733-9445(1999)125:4(372))
- Song, L.L. and Guo, T. (2017), “Probabilistic seismic performance assessment of self-centering prestressed concrete frames with web friction devices”, *Earthq. Struct., Int. J.*, **12**(1), 109-118. <https://doi.org/10.12989/eas.2017.12.1.109>
- Song, L.L., Guo, T. and Chen, C. (2014a), “Experimental and numerical study of a self-centering prestressed concrete moment resisting frame connection with bolted web friction devices”, *Earthq. Eng. Struct. Dyn.*, **43**(4), 529-545. <https://doi.org/10.1002/eqe.2358>
- Song, R., Li, Y. and van de Lindt, J.W. (2014b), “Impact of earthquake ground motion characteristics on collapse risk of post-mainshock buildings considering aftershocks”, *Eng. Struct.*, **81**, 349-361. <https://doi.org/10.1016/j.engstruct.2014.09.047>
- Song, L.L., Guo, T., Gu, Y. and Cao, Z.L. (2015a), “Experimental study of a self-centering prestressed concrete frame subassembly”, *Eng. Struct.*, **88**, 176-188. <https://doi.org/10.1016/j.engstruct.2015.01.040>
- Song, L.L., Guo, T. and Cao, Z.L. (2015b), “Seismic response of self-centering prestressed concrete moment resisting frames with web friction devices”, *Soil Dyn. Earthq. Eng.*, **71**, 151-162. <https://doi.org/10.1016/j.soildyn.2015.01.018>
- Tsai, K.C., Hsiao, C.P. and Bruneau, M. (2000), “Overview of building damages in 921 Chi-Chi earthquake”, *Earthq. Eng. Seismol.*, **2**(1), 93-108.
- USGS. (2018), U.S. geological survey. <http://www.usgs.gov/>
- Vasdravellis, G., Karavasilis, T.L. and Uy, B. (2013), “Large-scale experimental validation of steel post-tensioned connections with web hourglass pins”, *J. Struct. Eng.*, **139**(6), 1033-1042. [https://doi.org/10.1061/\(ASCE\)ST.1943-541X.0000696](https://doi.org/10.1061/(ASCE)ST.1943-541X.0000696)
- Xu, L.H., Fan, X.W. and Li, Z.X. (2016), “Development and experimental verification of a pre-pressed spring self-centering energy dissipation brace”, *Eng. Struct.*, **127**, 49-61. <https://doi.org/10.1016/j.engstruct.2016.08.043>
- Zhao, B., Taucer, F. and Rossetto, T. (2009), “Field investigation on the performance of building structures during the 12 May 2008 Wenchuan earthquake in China”, *Eng. Struct.*, **31**(8), 1707-1723. <https://doi.org/10.1016/j.engstruct.2009.02.039>

BU